ARTICLE

Remediation of Cu Contaminated Soil by $Fe_{78}Si_9B_{13}{}^{AP}$ Permeability Reaction Barrier Combined with Electrokinetic Method

Liefei Pei[1,2], Xiangyun Zhang[1] and Zizhou Yuan[1,*]

[1]School of Materials Science and Engineering, Lanzhou University of Technology, Lanzhou, China

[2]School of Mining and Metallurgy Engineering, Baiyin Mining and Metallurgy Vocational and Technical College, Baiyin, China

*Corresponding Author: Zizhou Yuan. Email: yuanzz@lut.edu.cn

ABSTRACT

Iron-based amorphous crystalline powder $Fe_{78}Si_9B_{13}{}^{AP}$ is used as a permeability reaction barrier (PRB) combined with an electrokinetic method (EK-PRB) to study the removal rate of Cu in contaminated soil. After treating Cu-contaminated soil for 5 days under different voltage gradients and soil water content, the soil pH is between 3.1 and 7.2. The increase of voltage gradient and soil water content can effectively promote the movement of Cu^{2+} to the cathode. The voltage gradient is 3 V/cm, and the water content of 40% is considered to be an optional experimental condition. Therefore, under this condition, the effects of $Fe_{78}Si_9B_{13}{}^{AP}$ and zero-valent iron (ZVI) as PRB on the removal rate of total Cu in soil and the transformation of chemical forms of Cu are studied. Compared with ZVI, $Fe_{78}Si_9B_{13}{}^{AP}$ as PRB has a better remediation effect. EK-$Fe_{78}Si_9B_{13}{}^{AP}$ can remove 80.3% of total Cu in soil, and the biologically available Cu is reduced to 3.6%, which effectively reduces the environmental risk of contaminated soil.

KEYWORDS

Soil contamination; amorphous alloy; electrokinetic method; immobilization

1 Introduction

Farmland soil is the home for human survival, which provides a guarantee for the sustainable development of human society. However, with the acceleration of the process of social industrialization, the waste gas, wastewater, and waste residue containing a variety of heavy metals produced in the process of industrial production are also immersed into the farmland soil, resulting in plant physiological function disorder and malnutrition [1,2]. And heavy metals are potentially harmful after entering the human body through the food chain. Studies have shown that excessive copper intake by biological weight will cause concentration differences on both sides of the plasma membrane, increase membrane lipid peroxidation and enhance permeability, resulting in the outflow of potassium ions required by plants out of the cell membrane, thus damaging the plasma membrane of plant roots [3–5]. In addition, high copper content in plants can inhibit the synthesis of amino acids, resulting in the inability of roots to grow and yellowing leaves [6,7]. Soil pollution has attracted more and more attention, and it has become an important environmental problem all over the world. Soil heavy metal pollution has become a research hotspot for environmental and soil scientists [8,9].

At present, the commonly used soil remediation methods include thermal desorption [10], solidification [11], leaching [12], electrokinetic [13], and microbial methods [14]. Among them, the electrokinetic method is a soil remediation technology that sprang up in the 1990s. Its principle is to apply a low-voltage electric field to the contaminated area, and the charged pollutants are enriched to the area near the electrode by the electrodynamic effects of the electric field, such as electroosmosis, electromigration, and electrophoresis. Then the soil in the enrichment area is centrally remediated by chemical immobilization, adsorption, leaching, and ion exchange [15,16]. This method is especially suitable for the treatment of farmland soil with fine particles and high water content, which has the advantages of simplicity, low cost, and excellent effect [17,18]. Huang et al. [19] used a mild electrokinetic method with a voltage gradient of 0.25 V/cm to treat cadmium-contaminated soil for 48 h, and the content of exchangeable cadmium is reduced by up to 72.3%, which effectively reduces the bioavailability of cadmium. In order to further optimize the remediation process of the electrokinetic method, some researchers proposed an electrokinetic method combined with PRB to remediate heavy metal-contaminated soil. Zhang et al. [20] compared the simple electrokinetic method with ZVI as PRB combined electrokinetic method (EK-ZVI) to remedy Pb, As, Cu and Zn contaminated soil. Under the action of electric field force, Pb^{2+}, As^{3+}, Cu^{2+}, and Zn^{2+} move to the cathode along the direction of the electric field, and the ion concentration increases gradually from the anode to the cathode. In the process of EK-ZVI combined remediation, near the PRB of ZVI, the concentrations of these four ions decreased due to the reduction of ZVI and the adsorption of iron oxides. However, the surface of ZVI is easy to be passivated, and its chemical activity is low, which seriously inhibits the immobilization effect of ions. Therefore, it is particularly important to develop new immobilized materials with high reaction activity.

Amorphous alloy (MGs) is a metastable material in which the superalloy melt solidifies rapidly at a cooling rate of more than 379 K/s. Its internal atoms are arranged in a long-range disorder and short-range order. This special atomic and electronic structure determines that MGs have higher chemical activity than crystalline materials in terms of catalytic performance [21]. Since the 1980s, some researchers have carried out theoretical research on the application of MGs to the degradation of environmental pollutants [22]. In recent years, a large number of literatures have reported the application of iron-based amorphous alloy (Fe-MGs) in the treatment of heavy metals and dye wastewater. For example, Tang et al. [23] compared the reaction rates k_{obs} of amorphous ribbon $Fe_{86}B_{14}{}^{AR}$, crystalline ribbon $Fe_{86}B_{14}{}^{CR}$, and ZVI in the treatment of wastewater contaminated by direct blue 6. The results show that under the same experimental conditions, the k_{obs} of the reaction of $Fe_{86}B_{14}{}^{AR}$ with direct blue 6 are 1.8 and 89 times higher than that of $Fe_{86}B_{14}{}^{CR}$ and ZVI, respectively, indicating that the ultra-high reaction activity of $Fe_{86}B_{14}{}^{AR}$ benefits from its unique amorphous structure. Yan et al. [24] used $Fe_{78}Si_9B_{13}{}^{AP}$ and ZVI to treat the wastewater, whose initial concentration of Cu^{2+} was 500 mg/L. After 1 h, the content of Cu^{2+} in the solution treated by $Fe_{78}Si_9B_{13}{}^{AP}$ was reduced to less than 1 mg/L, while the content of Cu^{2+} in the solution treated by ZVI still exceeds the upper limit of the discharge standard of industrial wastewater. Through Arrhenius formula fitting, it was found that the apparent activation energy of $Fe_{78}Si_9B_{13}{}^{AP}$ is only 1/2 times of that of ZVI. Zhang et al. [25] measured the valence band density of $Fe_{78}Si_9B_{13}{}^{AR}$ and ZVI, and found that the valence band top of $Fe_{78}Si_9B_{13}{}^{AR}$ moves down compared with ZVI, which leads to the corresponding broadening of the empty band of $Fe_{78}Si_9B_{13}{}^{AR}$. Therefore, the electrons in the 4 s orbital of the iron atom are easier to cross the top of the energy band into the empty band, thus causing a redox reaction with pollutants.

In view of the excellent performance of Fe-MGs in industrial wastewater treatment, this paper proposes for the first time to use $Fe_{78}Si_9B_{13}{}^{AP}$ instead of ZVI as PRB, combined with EK to remediate Cu-contaminated soil, focusing on the moving and immobilization process of Cu^{2+}. First of all, the best voltage gradient and soil water content were selected, and on this basis, EK-ZVI was compared to explore the mechanism of Cu removal and chemical transformation of EK-$Fe_{78}Si_9B_{13}{}^{AP}$ in soil. By observing the phase and morphology differences between $Fe_{78}Si_9B_{13}{}^{AP}$ and ZVI after the reaction, the internal mechanism of high reaction activity of $Fe_{78}Si_9B_{13}{}^{AP}$ is revealed.

2 Materials and Methods

2.1 Materials

The source of Cu in simulated contaminated soil is $CuSO_4 \cdot 5H_2O$. HCl and NaOH are used to regulate the initial pH of soil. 2% citric acid solution (CA) as cathode electrolyte. The chemicals used in the continuous extraction of soil include HCl, HNO_3, CH_3COONH_4, HOAc, $NH_2OH \cdot HCl$, H_2O_2, $HClO_4$. The above reagents are all analytically pure and are provided by Gansu ruidong Chemical products Co., Ltd. (Gansu China). The purity of $Fe_{78}Si_9B_{13}{}^{AP}$ and ZVI as PRB is more than 99.5%, and the average particle size is 30 μm, purchased from Beijing Yijin Chemicals Co., Ltd. (Beijing, China).

### 2.2 Soil Preparation

2.2.1 Soil Sampling

The loess soil of 5–10 cm underground without copper pollution was collected from the fields around Lanzhou University of Technology. After drying, the soil samples were screened with 2 mm sieve. The screened soil samples were washed three times with 0.1 mol/L HCl and distilled water to remove soluble salts and impurities. The washed soil is dried, ground, and then passed through the 2 mm sieve again.

2.2.2 Preparation of Cu-Contaminated Soil

The maximum copper content in the soil around the copper smelter of Baiyin Company (China), the largest copper producer in China, is 658 mg/kg [26]. As a result, it was determined that the total content of copper in the contaminated soil used in this experiment was 600 mg/kg. The operation is as follows: the spoon of 1 kg soil sample was gradually added to the $CuSO_4 \cdot 5H_2O$ solution of 1 L 600 mg/L, and the soil suspension was mechanically stirred until it was air-dried. In order to determine the uniformity of Cu dispersion in soil, different quality soil samples were added to the same volume of distilled water, and the content of Cu^{2+} was directly proportional to the added soil samples, which indicated that Cu dispersion in soil samples was good.

2.3 Experimental Device

The electric device used in this experiment was made of the corrosion-resistant glass plate. As shown in Fig. 1, the electric tank was divided into three parts by two pieces of the polytetrafluoroethylene filter membrane. The middle part was a soil chamber filled with Cu-contaminated soil, and its size was $170 \times 100 \times 100$ mm. On both sides were electrode chambers filled with KNO_3 solution. The soil chamber was flanked by electrode chambers. Two high-purity plate graphite electrodes ($100 \times 50 \times 4$ mm) connected to the DC power supply were inserted into the electrolyte solution to form a current path.
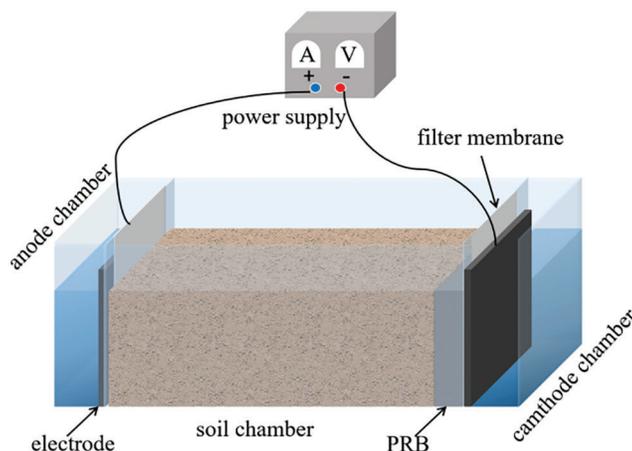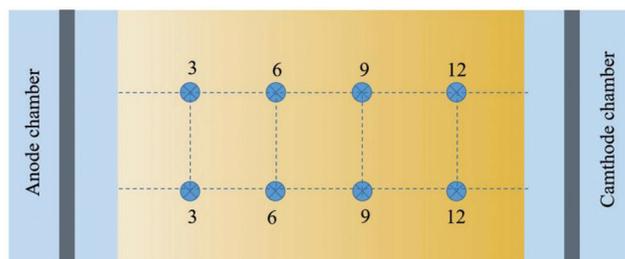

Figure 1: Schematic diagram of electrokinetic device

2.4 Electrokinetic Remediation

The electric remediation experiment was carried out in two stages. The first stage was the simple electrokinetic method without PRB, which explored the effects of water content, voltage gradient, and pH on the removal rate of total Cu in soil. The water content was set to 30%, 35%, 40%, and the voltage gradient was 1, 2, 3 V/cm. EK1-EK6 was carried out according to Table 1 to determine the optimal water content and voltage gradient. After the 1 kg contaminated soil samples were compacted in the electric reaction chamber, each group of experiments configured the soil solution according to the water content shown in Table 1. The soil chamber was covered with plastic film to prevent the evaporation of water. In order to transform the immobilized Cu into mobile Cu^{2+} as much as possible. The mixed solution of 0.05 mol/L citric acid and 0.1 mol/L $MgCl_2$ were used in the electrolyte. Fu et al. [27] have found that citric acid can effectively promote the electrokinetic process. After 12 h of balance, two plate graphite electrodes were vertically inserted into the anode and cathode electrode chamber and connected with wires to stabilize the DC power supply, and the corresponding voltage gradient was adjusted in each group of experiments. The electrolyte in the electrode chamber was changed regularly to avoid the OH^- generated by the cathode entering the soil during the electrolysis process and causing the focusing effect. Referring to the experimental cycle of the predecessors [28], it was determined that the electricity was stopped after 5 days of reaction, and the remedial soil was sampled. The sampling position is shown in Fig. 2, each sampling point was evenly spaced from anode to cathode, and 8 soil samples were taken from each reaction tank. According to the method introduced by Zhou et al. [29], the pH value and electrical conductivity of soil were measured by pH meter (PHS-3G) and electrical conductivity meter (ASAP-2010). In order to determine the total copper content at each sampling site, after each soil sample was digested with aqua regia, the concentration of Cu^{2+} was determined by an inductively coupled plasma atomic emission spectrometer (ICP-AES). The average extraction value of two soil samples in each column was taken as the experimental value. On the basis of the best combination determined by the first stage experiment, the second stage experiment was conducted with EK7 and EK8 to explore the morphological transformation of Cu and the change of total Cu content in soil when $Fe_{78}Si_9B_{13}^{AP}$ and ZVI were used as osmotic reaction barriers. Before the experiment, the crystal structure of $Fe_{78}Si_9B_{13}^{AP}$ was analyzed by Cu Kα irradiation (40 kV, 150 mA) X-ray diffractometer (XRD, Rigaku D/max-2400) and selected area electron diffraction (SAED) to ensure the amorphous structure of the powder. The operation procedure of these two groups of experiments was basically the same as that of the first stage, except that the infiltration PRB of $Fe_{78}Si_9B_{13}^{AP}$ and ZVI with a thickness of about 0.5 cm were embedded into the shade extreme of the soil chamber. After the reaction, each soil sample was continuously extracted according to the steps shown in Fig. 3 to determine the morphological transformation of Cu in the soil. XRD and SEM were used to analyze the phase composition and product morphology of $Fe_{78}Si_9B_{13}^{AP}$ and ZVI after the reaction.

Table 1: Experimental conditions of each group and average removal rate of Cu

Test number	Moisture content (%)	Voltage gradient (V/cm)	PRB	Average removal rate of Cu (%)
EK1	30	1		50
EK2	35	2		60.25
EK3	40	3		64.5
EK4	30	2		53.25
EK5	35	3		62.5
EK6	40	1		56.75
EK7	40	3	$Fe_{78}Si_9B_{13}^{AP}$	80.33
EK8	40	3	ZVI	69.25

Figure 2: Location of soil sampling sites (top view of electrokinetic device)
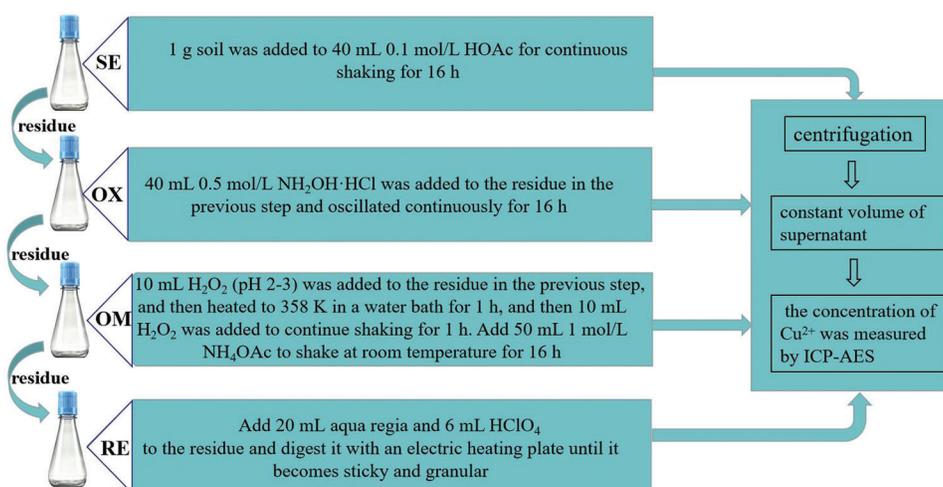

Figure 3: Continuous extraction steps of soil

3 Results and Discussion

3.1 Soil pH and Soil Conductivity

3.1.1 Soil pH

Fig. 4 shows the pH distribution of each sampling site after simple electrokinetic treatment of Cu-contaminated soil. On the whole, the pH of soil after remediation is significantly different from that before treatment, and the pH of each sampling site is also different. The initial pH of the soil is 6, and after 5 days of remediation, the soil pH changes to between 3.1 and 7.2. In each group of experiments, the pH increased gradually from anode to cathode. This is due to the electrolytic reaction of the water on the electrode in the electric remediation (anode: $2H_2O \rightarrow 4e^- + 4H^+ + O_2$, cathode: $2H_2O + 2e^- \rightarrow 2OH^- + H_2$), the H^+ produced by the anode and the OH^- produced by the cathode move in the opposite direction after entering the soil solution under the action of electric field force, and the concentrations of H^+ and OH^- are linearly distributed along the direction of the electric field. Some studies [30] have shown that the movement rate of H^+ is 1.8 times higher than that of OH^-, so the soil as a whole is in a slightly acidic environment and the acidity in the anode region is stronger than that in the cathode region. Compared with EK1 and EK6, it is found that the voltage gradient is 1 V/cm, the pH of the soil with 40% water content is 3.6, 4.6, 5.2, and 6.4, respectively, and the pH of the soil with 30% water content is 4, 5.8, 6.6, and 7, respectively. The pH of each sampling site in the soil with 40% water content is lower than that in the soil with 30% water content. Compared with EK2 and EK4, EK3 and EK5, there is a similar rule, which indicates that the soil with high water content has relatively low pH after being remedied by the electrokinetic method. This is due to the fact that more water in the soil with more water content is released by electrolysis to release H^+ and OH^-, and the acidity peak produced by H^+ in the soil

moves faster than the OH$^-$ alkaline peak, which increases the concentration difference between H$^+$ and OH$^-$ and enhances the acidity. When different voltage gradients are applied at both ends of the soil with the same water content, the effect on the soil pH of each sampling site is not obvious. Although the voltage gradient can change the movement rate of ions, it does not change the relative distribution of H$^+$ and OH$^-$ in soil.
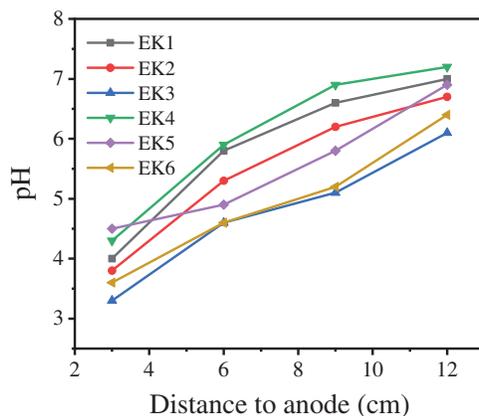
Figure 4: Soil pH at each sampling site

3.1.2 Soil Conductivity

Fig. 5 shows the electrical conductivity at different locations of the soil after electrokinetic remediation. The electrical conductivity cannot only reflect the number of free-moving ions in soil solution but also characterize the adsorption-desorption performance of soil to free ions to some extent. The conductivity of each point from the anode to the cathode decreases in turn, indicating that the number of free ions in the anode area is more than that in the cathode. This may be due to the weakening of the adsorption of ions by the soil under acidic conditions, and the ions are dissolved and released into the water. Therefore, the higher movement rate of the ions in the anode region is beneficial for the anode ions to move to the cathode region. Compared with EK1 and EK6, EK2 and EK4, EK3 and EK5, it is found that when the voltage gradient is the same, the number of free ions in the system with high water content is correspondingly higher. Compared with EK3 and EK6, EK2 and EK5, EK1 and EK4, it is found that when the water content is the same, the voltage gradient is positively correlated with electrical conductivity. It can be seen that higher water content and voltage gradient in the soil can inhibit the adsorption of ions in soil and promote the formation of free ions, which is conducive to the enrichment of heavy metal ions to the cathode region.
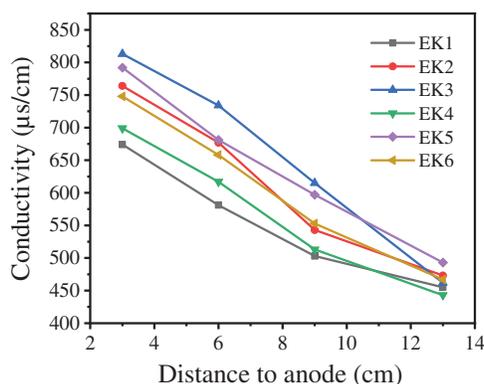
Figure 5: Soil electrical conductivity at each sampling site

3.2 The Removal Rate of Total Copper in EK1-EK6

Different water content and voltage gradient have a direct effect on the moving rate of Cu^{2+} in soil [31]. Fig. 6 shows the removal rate of total copper at each sampling point in EK1-EK6. Overall, the removal rate of Cu in the soil from anode to cathode decreased in turn. This is due to the electrical movement of the Cu^{2+} from the anode to the cathode along the direction of the electric field. A part of Cu^{2+} breaks away from the shackles of the soil and enters the cathode electrolytic chamber to pollute the electrolyte. The other part accumulates in the cathode region, thus forming a reverse electric field to inhibit the movement of Cu^{2+}. The average removal rate of total Cu in each group of experiments is shown in Table 1. In EK3, with maximum water content and maximum voltage gradient, the average removal rate of Cu is the highest, reaching 64.5%. On the contrary, the average removal rate of Cu in EK1 with minimum water content and voltage gradient is the lowest, only 50%. It shows that the increase of soil water content and voltage gradient is beneficial to the removal of Cu.
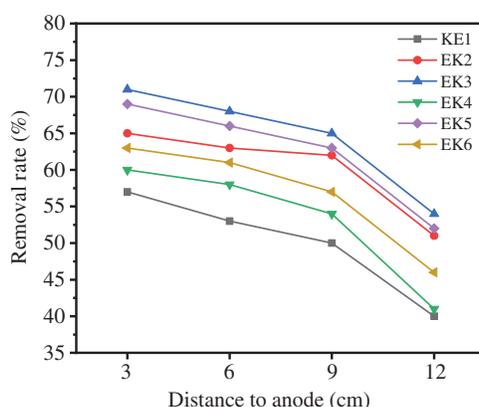
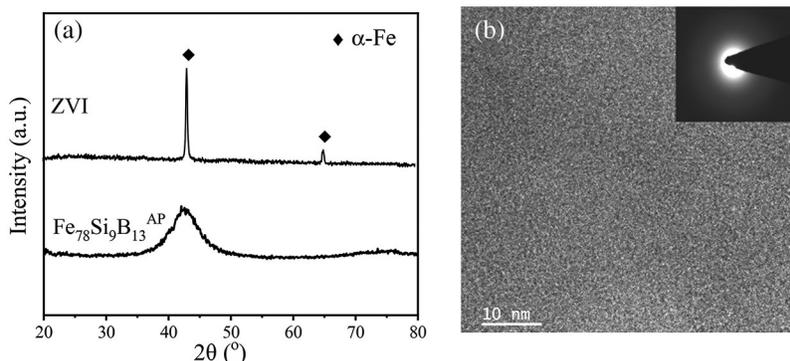**Figure 6:** The removal rate of total copper in EK1-EK6

3.3 Characterization of $Fe_{78}Si_9B_{13}{}^{AP}$ and ZVI

Fig. 7a shows the results of XRD analysis of $Fe_{78}Si_9B_{13}{}^{AP}$ and ZVI. The Bragg diffraction peak of crystal structure does not appear in the diffraction pattern of $Fe_{78}Si_9B_{13}{}^{AP}$, but shows a broadening uplift in the range of $2\theta = 40$–$60°$, indicating that the atomized powder is mainly amorphous. The crystallization peak of α-Fe phase is observed in the ZVI pattern, while that of other impurities is not observed in other places, indicating that the purity of ZVI is higher and the surface oxide is less. There are no lattice stripes in the TEM image of $Fe_{78}Si_9B_{13}{}^{AP}$ (Fig. 7b), and the atoms are arranged uniformly and disorderly. The illustration SAED image is the diffraction halo of $Fe_{78}Si_9B_{13}{}^{AP}$. Combined with the analysis results of XRD, it can be determined that the $Fe_{78}Si_9B_{13}{}^{AP}$ used is amorphous.

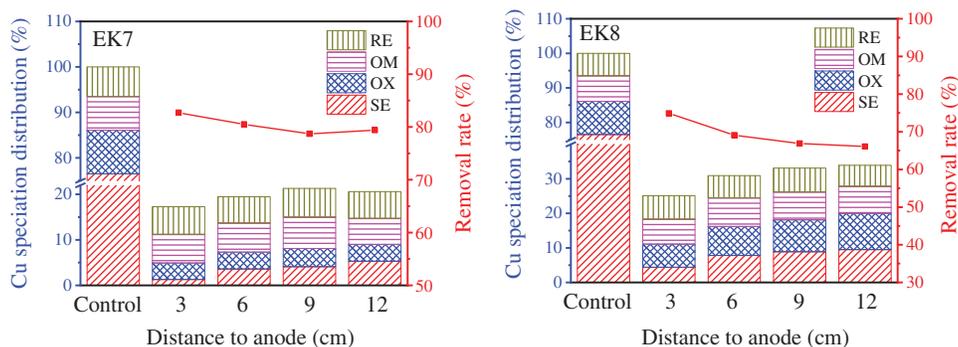### 3.4 Speciation Distribution of Copper and Removal Rate of Total Copper in EK7 and EK8

As can be seen from the experimental results of 3.2, it is difficult to achieve the ideal effect of using the electrokinetic method to remedy heavy metal-contaminated soil. In order to eliminate the inhibitory effect of positive ions accumulated in the cathode region on the movement of Cu^{2+} in time, EK7 and EK8 used $Fe_{78}Si_9B_{13}{}^{AP}$ and ZVI as PRB to improve the removal rate of Cu in soil. In addition, heavy metals can combine with different components in the soil to form a variety of chemical forms, and their chemical forms affect the movement rate and transformation process of heavy metals in the soil, as well as the toxicity to organisms and the degree of influence on the environment [32]. The three-stage BCR sequential extraction [33] divides the heavy metals in soil into the soluble, exchangeable state (SE), reducible state (OX), oxidizable state (OM), and residual state (RE). Among them, SE has strong

mobility and transformation, which can easily enter the organism and interfere with the normal metabolic activities of organisms, so the environmental risk level of SE is the highest. Most soil remediation methods are to reduce the content of SE. OX, OM, and RE are called stationary states, and these heavy metals are difficult to move and transform. Therefore, the environmental risk level of these three forms is lower than that of SE.

Figure 7: (a) The XRD spectra morphology of the $Fe_{78}Si_9B_{13}{}^{AP}$ and ZVI before reaction; (b) The TEM image of the $Fe_{78}Si_9B_{13}{}^{AP}$

Fig. 8 shows the chemical form distribution of copper and the removal rate of total copper after using $Fe_{78}Si_9B_{13}{}^{AP}$ (EK7) and ZVI (EK8) as PRB to remediate Cu-contaminated soil by electrokinetic method for 5 days. Before remediation, Cu existed mainly as SE in the soil, accounting for about 76% of the total copper content. The contents of OM, OX, and RE are relatively less. It shows that the environmental risk level of Cu-contaminated soil is very high, so it is necessary to carry out reasonable remediation. The total copper content of all sampling sites in EK7 and EK8 decreased, and the total copper content from anode to cathode in EK7 gradually decreased to 82.7%, 80.5%, 78.7% and 79.4%, respectively. Taking the average removal rate of each point, the removal rate of Cu is 80.3%. However, the removal rates of EK8 are lower than that of EK7, which are 74.9%, 69.1%, 66.9%, and 66.1%, respectively. The average removal rate of Cu is only 69.2%. It can be seen that different materials of PRB have an obvious influence on the movement and removal of Cu. Some researchers have confirmed that the reaction rate of $Fe_{78}Si_9B_{13}{}^{AP}$ with Cu^{2+} is 167 times that of ZVI [34]. Therefore, the Cu^{2+} moving from the anode region to the cathode is rapidly reduced and precipitated from the solution by $Fe_{78}Si_9B_{13}{}^{AP}$, which eliminates the reverse potential formed by the accumulation of Cu^{2+} in time, and promotes the continuous movement of Cu^{2+} to the cathode. On the contrary, the reaction rate between ZVI and Cu^{2+} is slower, and the accumulation of Cu^{2+} in the cathode region inhibits the movement of Cu^{2+} in the anode region to some extent.

**Figure 8:** With $Fe_{78}Si_9B_{13}{}^{AP}$ (EK7) and ZVI (EK8) as PRB and electrokinetic remediation of Cu-contaminated soil for 5 days, copper speciation distribution and total copper removal rate were studied

Comparing the chemical form changes of Cu before and after remediation, it is found that the content of SE decreases significantly in both groups. The SE content of each sampling point from anode to cathode in EK7 is 3.6%, 3.7%, and 3.7%, respectively, while the SE content of EK8 from anode to cathode is 4.4%, 7.8%, 8.9% and 9.5%, respectively. By comparison, it is found that SE in EK8 is slightly higher than EK7. The result proves once again that $Fe_{78}Si_9B_{13}{}^{AP}$ has higher reactivity than ZVI and can immobilize Cu^{2+} through reduction more thoroughly. The OX content in the anode area is slightly lower than that before remediation, which is due to the enhancement of acidity in the anode area with the progress of electrokinetic process, resulting in the release of some Cu combined with Fe-Mn oxides. Because it is difficult to transform Cu into OM and RE in a short period of time, the contents of these two parts remain basically unchanged, indicating that the electric remediation method has little damage to soil organic matter and soil lattice. According to the above experimental results, the soil remediated by EK7 and EK8 is in full compliance with the "Soil Environmental Quality Risk Control Standard for Soil Contamination of Development" [35].

3.5 Reaction Mechanism Analysis

Generally speaking, soil particles have a negative charge and can adsorb heavy metal ions with a positive charge. Therefore, it is difficult to remove it by direct elution. If a constant voltage electric field is applied at both ends of the contaminated soil, the heavy metal ions will not only dissolve, precipitate, and self-diffuse but also move and permeate under the action of the electric field force. Thus the adsorption force of the soil can be overcome and separated from the soil [36]. The removal mechanism of Cu^{2+} in the soil system is shown in Fig. 9. Under the above forces, electric movement and electroosmosis are the main factors that Cu^{2+} can be analyzed from the soil. Under the action of electric field force, Cu^{2+} moves from the anode to the cathode in the direction of the electric field and is reduced and immobilized in PRB. In the process of electrokinetic reaction, the OH^- produced by the electrolytic reaction of water in the cathode combines with H^+ in citric acid, and the excess OH^- is moved to PRB or soil by electroosmosis to increase the pH in the cathode region. As the alkaline environment is not conducive to the movement of Cu^{2+}, it is necessary to replace the cathode electrolyte regularly.
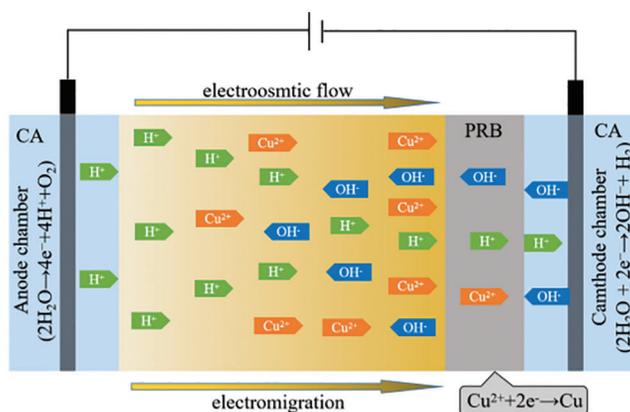

Figure 9: The main mechanism of Cu^{2+} removal in an electric system

Because the H^+ produced by the anode moves faster to the cathode than OH^-, most of the soil near the anode is acidic, which is beneficial to the analysis and movement of Cu^{2+}. Therefore, the removal rate of Cu^{2+} in the anode area is higher than that in the cathode area. In order to eliminate the accumulation of Cu^{2+} in the cathode area and improve the removal rate of Cu in the cathode area. In this experiment, $Fe_{78}Si_9B_{13}{}^{AP}$ with higher chemical reaction activity was selected as the PRB material, and the Cu^{2+}

moved to the cathode was reduced in time, which eliminated the inhibitory effect of the reverse electric field on the movement of Cu^{2+}.

In order to further explore the internal mechanism that $Fe_{78}Si_9B_{13}{}^{AP}$ has high reaction activity, the $Fe_{78}Si_9B_{13}{}^{AP}$ and ZVI after reaction are analyzed by XRD and SEM. From the XRD spectra of the products of the $Fe_{78}Si_9B_{13}{}^{AP}$ and ZVI in Fig. 10, it can be seen that the Bragg diffraction peak of Cu^0 is superimposed on the broadened amorphous diffraction peak on the spectral line of $Fe_{78}Si_9B_{13}{}^{AP}$, indicating that the reduced product of Cu^{2+} is immovable Cu^0, and the reaction only takes place on the surface of $Fe_{78}Si_9B_{13}{}^{AP}$, which ensures the continuous and efficient reaction. The crystallization peak of Cu^0 also appears in the XRD spectrum of the ZVI, indicating that the two kinds of iron-based materials can effectively reduce and immobilize Cu^{2+}. From the standard electrode potentiometer, it is known that the standard electrode potential $E(Cu/Cu^{2+})$ of copper is higher than the standard electrode potential $E(H_2/H^+)$ of hydrogen, so changing the cathodic electrolyte will not cause the secondary dissolution of immobilized Cu^0. XRD analysis shows that the reduction reaction takes place on the surface interface of the powder, so the morphology of the product will have a direct effect on the reaction rate. Fig. 11 shows the difference of the surface morphology of the products after the reaction of $Fe_{78}Si_9B_{13}{}^{AP}$ and ZVI. From Fig. 11a, it is observed that spherical microcrystals of different sizes are produced on the surface of $Fe_{78}Si_9B_{13}{}^{AP}$, and a large number of unspheroidal lamellar structures appear in other regions. Through the high-resolution image of Fig. 11b, it is found that there are a large number of nano-lamellar intercalated pore structures perpendicular to the sphere in these regions, and Cu^{2+} can be diffused to the reaction interface through the channels, which is conducive to the sustainability of the reaction. Combined with the literature [37], it is known that the shedding mode of the $Fe_{78}Si_9B_{13}{}^{AP}$ product layer is to form a lamellar structure intercalated with each other on the surface, and these lamellae grow up gradually to form spherical microcrystals. When the spherical microcrystal grows to a certain size, it falls off from the surface of $Fe_{78}Si_9B_{13}{}^{AP}$, so that the powder always maintains a thin product layer. In order to determine the material composition of these nano-lamellar structures, the elemental scanning analysis of the e region in the figure shows that the surface element ratio is Cu:Fe:Si:B = 73.4:23.6:2.1:0.9 in Fig. 11e. It can be seen that the main component of the product is Cu, and some iron oxides are attached. At the same time, lower contents of Si et al. [38] found that Si and B are oxidized to form SiO_2 and B_2O_3, and the volume expansion makes the product layer easy to detach from the powder surface, which is one of the reasons why $Fe_{78}Si_9B_{13}{}^{AP}$ has high reaction activity. Fig. 11c shows that there are small and uniform spherical microcrystals on the surface of ZVI, which are difficult to grow and fall off and can only be closely covered on the surface of the powder. The high-resolution image of Fig. 11d also found that there is a layer of flocculent film on the outer surface of the product layer, which is mainly composed of Cu (78.5%) and Fe (21.5%), which hinders the mass transfer process of the reaction and reduces the chemical reaction rate. Cao et al. [39] believed that the difference in the morphology of the products on the surface of the amorphous structure and crystal structure is caused by the existence of an active "liquid-like" layer on the surface of the amorphous structure. In addition, Tang et al. [40] compared the reaction rate of amorphous ribbon Fe-Si-B^{AR} and crystalline ribbon Fe-Si-B^{CR} with methyl orange under the same conditions and found that the reaction rate of Fe-Si-B^{AR} is 26 times higher than that of Fe-Si-B^{CR}, indicating that the amorphous structure can effectively improve the reaction activity of Fe-Si-B^{AR}.
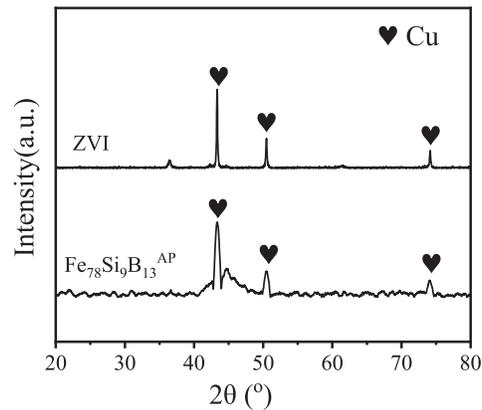
Figure 10: XRD spectra of the products of the $Fe_{78}Si_9B_{13}^{AP}$ (EK7) and ZVI (EK8)

In a word, the analysis of the mechanism of high reaction activity of Fe-based amorphous alloys and the existing literature reports are summarized as follows: (1) Compared with crystalline alloys. Amorphous alloys have lower activation energy and less energy for the chemical reaction [41]. (2) Fe-based amorphous alloys have more negative redox potential than amorphous alloys, which increases the driving force of electron transfer [40]. (3) The downward shift of the valence band top of the Fe-based amorphous alloy makes it easier for the valence electrons from the 4 s electron shell to overcome the energy barrier and be activated, thus crossing the valence band top into the empty band to participate in the formation of new materials [25].
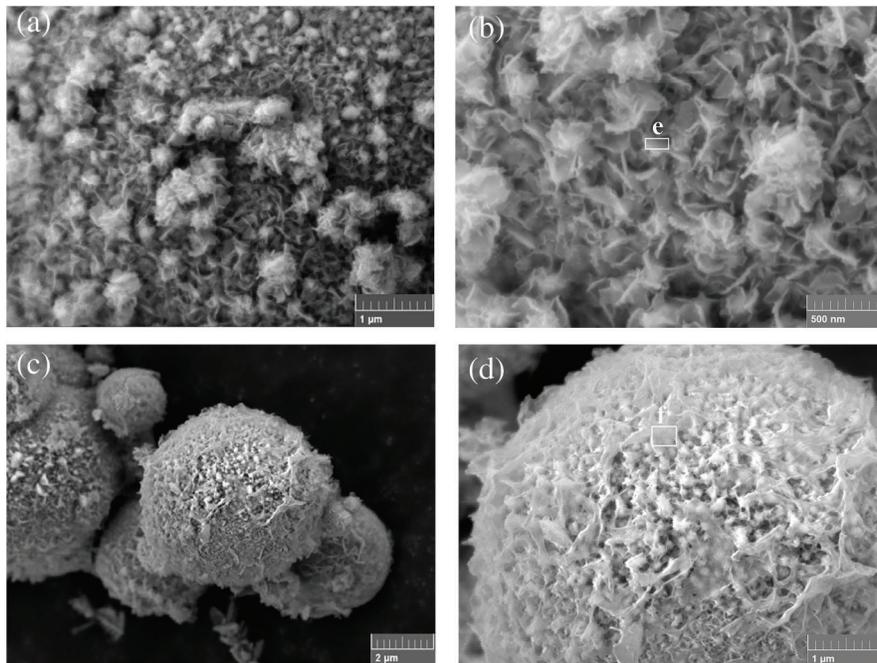
Figure 11: (Continued)
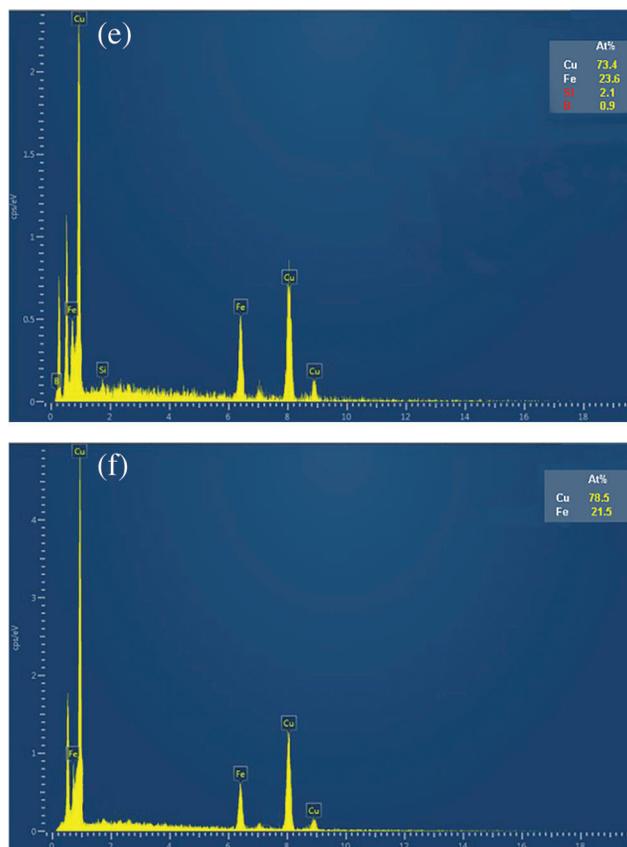
Figure 11: (a) The morphology of $Fe_{78}Si_9B_{13}{}^{AP}$ surface after reaction; (b) High-resolution map of (a); (c) The morphology of ZVI surface after reaction; (d) High-resolution map of (c); (e) The element content of area e in (b); (f) The element content of area f in (d)

4 Conclusions

The EK-$Fe_{78}Si_9B_{13}{}^{AP}$ remediation process developed in this study can effectively remove total Cu and movable Cu in soil. The increase of soil water content and voltage gradient can significantly improve the mobility of Cu. When there is no PRB, the water content is 40%, and the voltage gradient is 3 V/cm, the average removal rate of Cu is 64.5%. When $Fe_{78}Si_9B_{13}{}^{AP}$ and ZVI are added as PRB, the average removal rate of Cu reaches 80.3% and 69.2%, respectively, and the content of movable copper decreases to 3.6% and 4.4%, respectively. Compared with ZVI, $Fe_{78}Si_9B_{13}{}^{AP}$ as PRB can quickly immobilize Cu^{2+} that moves to the cathode region. As a result, the bioavailable Cu in the soil can be effectively removed, and the environmental risk grade of contaminated soil can be reduced.

Conflicts of Interest: The authors declare that they have no conflicts of interest to report regarding the present study.

References

1. Shang, E., Xu, E., Zhang, H., Huang, C. (2019). Temporal-spatial trends in potentially toxic trace element pollution in farmland soil in the major grain-producing regions of China. *Scientific Reports, 9(1),* 19463. https://doi.org/10.1038/s41598-019-55278-5

2. Zeng, S. Y., Ma, J., Yang, Y., Zhang, S. L., Liu, G. J. et al. (2019). Spatial assessment of farmland soil pollution and its potential human health risks in China. *Science of the Total Environment, 687(15),* 642–653. https://doi.org/10.1016/j.scitotenv.2019.05.291

3. Baryla, A., Laborde, C., Montillet, J. L. (2000). Evaluation of lipid peroxidation as a toxicity bioassay for plants exposed to copper. *Environmental Pollution, 109(1),* 131–135. https://doi.org/10.1016/S0269-7491(99)00232-8

4. Lei, X., Xing, X., Liang, J., Peng, J., Jing, Z. (2019). *In situ* phytoremediation of copper and cadmium in a co-contaminated soil and its biological and physical effects. *RSC Advances, 9(2),* 993–1003. https://doi.org/10.1039/C8RA07645F

5. Li, J., Qiu, Y., Zhao, Q., Chen, D., Wu, W. (2020). Lead and copper-induced hormetic effect and toxicity mechanisms in lettuce (*Lactuca sativa* L.) grown in a contaminated soil. *Science of the Total Environment, 741,* 140440. https://doi.org/10.1016/j.scitotenv.2020.140440

6. Weber, M. B., Schat, H., Maarel, B. V. D. (1991). The effect of copper toxicity on the contents of nitrogen compounds in *Silene vulgaris* (Moench) garcke. *Plant and Soil, 133(1),* 101–109. https://doi.org/10.1007/BF00011904

7. Napoli, M., Cecchi, S., Grassi, C., Baldi, A., Zanchi, C. A. (2019). Phytoextraction of copper from a contaminated soil using arable and vegetable crops. *Chemosphere, 219,* 122–129. https://doi.org/10.1016/j.chemosphere.2018.12.017

8. Zhang, J., Xu, Y., Wu, Y., Hu, S., Zhang, Y. (2019). Dynamic characteristics of heavy metal accumulation in the farmland soil over Xiaoqinling gold-mining region, Shaanxi, China. *Environmental Earth Sciences, 78(1),* 1–11. https://doi.org/10.1007/s12665-018-8013-2

9. Tao, Y., Huang, H., Zhang, H. (2020). Remediation of Cu-phenanthrene co-contaminated soil by soil washing and subsequent photoelectrochemical process in presence of persulfate. *Journal of Hazardous Materials, 400(8),* 123111. https://doi.org/10.1016/j.jhazmat.2020.123111

10. Liu, H., Li, J., Zhao, M., Li, Y., Chen, Y. (2019). Remediation of oil-based drill cuttings using low-temperature thermal desorption: Performance and kinetics modeling. *Chemosphere, 235.* 1081–1088. https://doi.org/10.1016/j.chemosphere.2019.07.047

11. Rattanapan, C., Sawain, A., Suksaroj, T., Chaisri, S. (2011). Enhanced efficiency of dissolved air flotation for biodiesel wastewater treatment by acidification and coagulation processes. *Desalination, 280(1–3),* 370–377. https://doi.org/10.1016/j.desal.2011.07.018

12. Someya, M., Higashino, K., Imoto, Y., Sakanakura, H., Yasutaka, T. (2020). Effects of membrane filter material and pore size on turbidity and hazardous element concentrations in soil batch leaching tests. *Chemosphere, 265(1–6),* 128981.

13. Mohamadi, S., Saeedi, M., Mollahosseini, A. (2020). Enhanced electrokinetic remediation of mixed contaminants from a high buffering soil by focusing on mobility risk. *Journal of Environmental Chemical Engineering, 7(6),* 103470. https://doi.org/10.1016/j.jece.2019.103470

14. Toan, Q. D., Mengke, W., Tran, T., Zhou, F., Wang, D. et al. (2019). Bioavailability of selenium in soil-plant system and a regulatory approach. *Critical Reviews in Environmental Science and Technology, 49(6),* 443–517. https://doi.org/10.1080/10643389.2018.1550987

15. Behrouzinia, S., Ahmadi, H., Abbasi, N., Javadi, A. A. (2021). Insights into enhanced electrokinetic remediation of copper-contaminated soil using a novel conductive membrane based on nanoparticles. *Environmental Geochemistry and Health, 73,* 1–18.

16. Vizcaíno, R., Yustres, A., Asensio, L., Saez, C. (2018). Enhanced electrokinetic remediation of polluted soils by anolyte pH conditioning. *Chemosphere, 199,* 477–485. https://doi.org/10.1016/j.chemosphere.2018.02.038

17. Salihu, L., Hussain, E. M., Dalhat, M. N., Alaadin, B., (2013). Coupled electrokinetics-adsorption technique for simultaneous removal of heavy metals and organics from saline-sodic soil. *Scientificworldjournal, 2013,* 346910.

18. Reddy, K. R. (2010). Technical challenges to in-situ remediation of polluted sites. *Geotechnical & Geological Engineering, 28(3),* 211–221. https://doi.org/10.1007/s10706-008-9235-y

19. Huang, B., Chi, G., Chen, X., Shi, Y. (2017). Mild electrokinetic treatment of cadmium-polluted manure for improved applicability in greenhouse soil. *Environmental Science & Pollution Research, 24(5),* 24011–24018. https://doi.org/10.1007/s11356-017-0058-3

20. Zhang, Y., Peng, Y. (2017). Research on zero valent iron PRB combined electrokinetic remediation of multi-metals contaminated farmland soil. *Guangdong Chemical Industry, 44(12),* 318–319.

21. Tong, X., Wang, G., Stachurski, Z. H., Mattern, N., Zhai, Q. J. et al. (2016). Structural evolution and strength change of a metallic glass at different temperatures. *Scientific Reports, 6.* 386–474.

22. Baiker, A. (1989). Metallic glasses in heterogeneous catalysis. *Faraday Discussions of the Chemical Society, 87,* 239–251.

23. Tang, Y., Shao, Y., Chen, N., Yao, K. F. (2014). Rapid decomposition of direct blue 6 in neutral solution by Fe-B amorphous alloys. *RSC Advances, 5(8),* 6215–6221.

24. Yan, Y., Liang, X., Ma, J., Shen, J. (2020). Rapid removal of copper from wastewater by Fe-based amorphous alloy. *Intermetallics, 124,* 106849.

25. Zhang, C. Q., Zhu, Z. W., Zhang, H. F., Hu, Z. Q. (2011). Rapid reductive degradation of azo dyes by a unique structure of amorphous alloys. *Chinese Science Bulletin, 56(36),* 3988–3992.

26. Zhao, B. W., Wang, G. (2010). Preliminary investigation and assessment of farmland soils contaminated by heavy metal around Baiyin City. *Environmental Science & Technology, 33(11),* 79–81.

27. Fu, R., Wen, D., Xia, X., Zhang, W., Gu, Y. (2017). Electrokinetic remediation of chromium (Cr)-contaminated soil with citric acid (CA) and polyaspartic acid (PASP) as electrolytes. *Chemical Engineering Journal, 316,* 601–608.

28. Zhao, S., Fan, L., Zhou, M., Zhu, X., Li, X. (2016). Remediation of copper contaminated kaolin by electrokinetics coupled with permeable reactive barrier. *Procedia Environmental Sciences, 31,* 274–279.

29. Zhou, H., Liu, Z., Li, X., Xu, J. (2020). Remediation of lead (II)-contaminated soil using electrokinetics assisted by permeable reactive barrier with different filling materials. *Journal of Hazardous Materials, 408,* 124885.

30. Yuan, C., Chiang, T. S. (2007). The mechanisms of arsenic removal from soil by electrokinetic process coupled with iron permeable reaction barrier. *Chemosphere, 67,* 1533–1542.

31. Zulfiqar, W., Iqbal, M. A., Butt, M. K. (2016). Pb^{2+} ions mobility perturbation by iron particles during electrokinetic remediation of contaminated soil. *Chemosphere, 169,* 257–261. https://doi.org/10.1016/j.chemosphere.2016.11.083

32. Attaeian, B., Mortazavi, S., Farokhzadeh, B., Khorsand, M. (2019). Evaluation and mapping satial distribution of copper pollution in soil and water of vineyard garden. *Journal of Environmental Health Engineering, 6(3),* 293–310. https://doi.org/10.29252/jehe.6.3.293

33. Davidson, C. M., Duncan, A. L., Littlejohn, D., Ure, A. M., Garden, L. M. (1998). A critical evaluation of the three-stage BCR sequential extraction procedure to assess the potential mobility and toxicity of heavy metals in industrially-contaminated land. *Analytica Chimica Acta, 363(1),* 45–55. https://doi.org/10.1016/S0003-2670(98)00057-9

34. Zhang, X., Liu, J., Li, J., Li, C. Y., Yuan, Z. Z. (2020). Excellent capability in remediating Cu^{2+} from aqueous solution by Fe-Si-B amorphous alloys. *Applied Physics A, 126(4),* 291–230. https://doi.org/10.1007/s00339-020-3465-0

35. Soil environmental quality risk control standard for soil contamination of development land. GB36600–2018. http://www.mee.gov.cn/ywgz/fgbz/bz/bzwb/trhj/201807/t20180703_446027.shtml

36. Li, C., Hou, H., Yang, J., Liang, S., Shi, Y. et al. (2019). Comparison of electrokinetic remediation on lead-contaminated kaolinite and natural soils. *Clean-Soil Air Water, 47,* 1800337. https://doi.org/10.1002/clen.201800337

37. Chen, S. Q., Dong, L. Z., Hui, K. Z., Zhen, P., Li, Z. et al. (2018). Fe-based multi-phase nanocrystalline ribbons with hierarchically flowerlike structured metal oxides after modified by orange II for Cr VI absorption. *Journal of Iron and Steel Research International, 25(6),* 608–613. https://doi.org/10.1007/s42243-018-0086-3

38. Jia, Z., Duan, X., Zhang, W., Wang, W., Aun, H. et al. (2016). Ultra-sustainable $Fe_{78}Si_9B_{13}$ metallic glass as a catalyst for activation of persulfate on methylene blue degradation under UV-Vis light. *Scientific Reports, 6(1),* 1–10. https://doi.org/10.1038/srep38520

39. Cao, C. R., Huang, K. Q., Shi, J. A., Zheng, D. N., Wang, W. H. et al. (2019). Liquid-like behaviours of metallic glassy nanoparticles at room temperature. *Nature Communications, 10(1),* 1–8. https://doi.org/10.1038/s41467-019-09895-3

40. Tang, Y., Shao, Y., Chen, N., Liu, X. (2015). Insight into the high reactivity of commercial Fe–Si–B amorphous zero-valent iron in degrading azo dye solutions. *RSC Advances, 5(43),* 34032–34039. https://doi.org/10.1039/C5RA02870A

41. Wang, J. Q., Liu, Y. H., Chen, M. W., Louzguine, L. D. V., Lnoue, A. P. J. H. (2012). Excellent capability in degrading azo dyes by MgZn-based metallic glass powders. *Scientific Reports, 2(1),* 1–6. https://doi.org/10.1038/srep00418